Study of Novel High Field Magnetic Resonance Imaging Traveling Wave System

By

Yue Li

B.S. Electrical and Computer Engineering

Submitted to

The College of Engineering in fulfillment of the requirements of

B.S. Honors with Research Distinction

In

Electrical and Computer Engineering

Thesis Advisor: Prof. Roberto G. Rojas

Final Exam Committee Member: Prof. Petra Schmalbrock

The Ohio State University

Spring 2013

Table of Contents

1.0 Introduction

The main challenge of high field strength conventional Magnetic Resonance Imaging (MRI), as a means of high quality medical imaging without ionizing radiation, is to maintain a homogeneous field excitation [1].

Recently, a new mode of operation based on traveling electromagnetic (EM) waves has been introduced. A patch antenna instead of the usual RF coil has been utilized to transmit radio-frequency signals. This technique applies the theory of waveguides and travelling waves at RF frequencies. The first step to optimize this new imaging scheme will be to determine the optimal waveguide modes based on the imaging application. Once these modes are determined, they have to be strongly excited in the cylindrical structure of the MRI with an appropriately designed waveguide exciters. An exciter, similar to the well-known microstrip antenna was recently built and tested on a Philips 7 Tesla MRI scanner at OSU; however, the images obtained had unsatisfactory signal-to noise ratios.

In this study, a complete computer model of a traveling wave MRI has been built and used to understand the key mechanisms of this novel imaging method. Preliminary calculations of the propagation and evanescent modes can be used in the future optimum design of the waveguide exciter.

2.0 Background and Motivation

Although MRI has been an outstanding means of medical imaging for the last three decades, concepts to increase the quality of the MRI signals by increasing the magnetic field strength have been proposed. To achieve homogenous excitation fields (B1), Hernandez [1], under the supervision of Profs. Rojas and Schmalbrock, tested the traveling wave MRI technique, a new approach to enhance the quality of B1 distributions and obtain better quality images from higher field MRI scanners. Currently, 3D gradient-echo sequence (GRE) scans using two flip angles and 2D GRE scans at various flip angles are utilized to measure B1distributions and phantom's T1 value [1]. Moreover, instead of a linearly polarized mode, a circularly polarized (CP) wave (Figure 1) will be excited in the cylindrical bore of the scanner. CP waves can reduce standing waves which can result in image distortion [2].

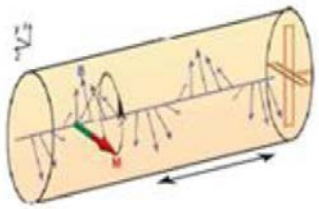

Figure 1: Propagation of circularly polarized wave in bore of MRI [2]

In addition, the bore acts as a waveguide for RF waves, which can propagate only above their respective cutoff frequencies. For the 7 Tesla MRI scanner, the lowest order mode, assuming the scanner is empty (no phantom), will propagate for frequencies above 298 MHz [2]. The Department of Radiology at OSU is one of few ultra-high field MRI centers. It recently acquired

a Philips 7 Tesla Magnetic Resonance Imaging Systems (Figure 2) in its new Weight Center of Innovation in Biomedical Imaging [3].

Figure 2: Philips 7 Tesla Magnetic Resonance Imaging System at OSU

Hernandez [1] tested a 350-mm-diameter patch antenna (Figure 3) in the 7-T MRI scanner to image a T-Shaped PVC pipe and a Human Torso shaped phantom filled with a solution consisting of 50% water, 49% sugar and 1% salt. However, a weak relation between traveling wave phase variability and frequency/phase encoding was observed. This can degrade image quality and hence, an optimized waveguide exciter needs to be redesigned.

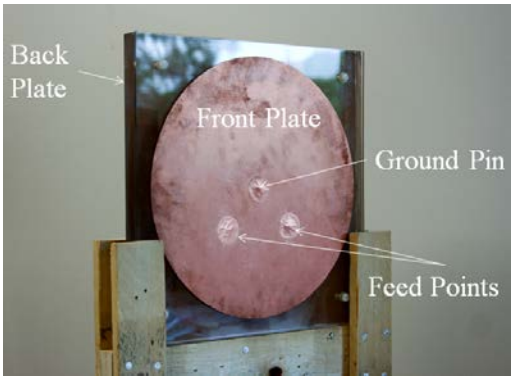

Figure 3: Current 350-mm-diameter patch antenna at OSU [1]

3.0 Problem Statement

Although some preliminary work has been done in this topic, there are a number of issues that need to be studied more carefully to fully understand how the traveling wave MRI works, and what can be done to improve its performance. The proposed research will develop a computer model for a traveling wave MRI so that waveguide exciters (antennas) can be redesigned and optimized.

More specifically, the model for the current 350-mm-diameter patch antenna was developed with the help of ANSYS HFSS, a tool for 3-D full-wave electromagnetic field simulation, to investigate its input impedance and radiation properties in free space, in an empty waveguide as well as in a waveguide with a phantom. After the numerical solution is obtained with HFSS, the data, including S-parameters for the antennas as well as the near or far fields of the antenna, can be exported to other software for additional processing. For example, the S parameters generated by HFSS can be exported to ADS (Advanced Design System). In ADS, these data can be converted, if desired, to Z parameters. The two-port S-parameters can be compared with measured two-port S-parameter data of the antenna. In this study, the S-parameters were combined with a 3dB hybrid coupler to generate two signals of equal magnitude and 90 degree out of phase (phase quadrature). This is necessary because the antenna is circularly polarized and needs to be fed by two signals of equal amplitude and 90 degree out of phase. The one port S-parameter or input impedance can then be compared with experimental data where a 3dB hybrid coupler is also used.

Additionally, the empty waveguide modes (propagating and evanescent, as well as their corresponding cut-off frequencies) can be calculated in closed from for the given dimensions of the MRI tube for a range of RF frequencies. To calculate the excitation coefficents of each of

these modes when the microstrip antenna is the exciter, it is necessary to first determine the near fields of the antenna when it is located in the MRI bore. This is accomplished in HFSS and the data is exported to Matlab. In Matlab, the excitation coefficients are obtained numerically. This calculation allows us to determine which modes are excited strongly and which ones are not. These results can be used in COMSOL where it is possible to model the MRI bore with a phantom and a strong DC magnetic field. Note that this is not possible to do in HFSS. However, this software (COMSOL) has a limitation; namely, we can only chose one of the waveguide modes as the incident mode. Therefore, the software does not allow us to use the antenna as the exciter. Fortunately, we can overcome this limitation by calculating all the excitation coefficients in Matlab. To summarize, this work will help future researchers model the MRI with a strong DC magnetic field and a phantom where the modes are excited by an antenna (exciter). COMSOL is, a finite-element based differential equation solver, to allow us to study the propagation of electromagnetic waves within a waveguide filled with gyrotropic materials.

4.0 Design and Results

Based on the current 350-mm-diameter patch antenna, a computer model (Figure 4) was built with HFSS to determine its input impedance behavior and radiation properties, including near and far-field calculations. It consists of a copper ground plane (40.64cm*40.64cm*1mm) and two plexiglass plates (40.64cm*40.64cm *5mm and 40.64cm*40.64cm *25mm thick) with air gap (0.2cm) in between. The front plate is a circular copper patch (35-mm-diameter) with a ground pin in the center to connect to the ground plane. The feed points inside the antenna are simulated as two perfect electrical conductors (PEC). Outside of the antenna, vacuum cylinders, with perfect electrical surfaces surrounding the perfect electrical conductor, have been used to simulate the coaxial connectors. At the terminal of each feed point, a plug is utilized to absorb the energy coming back to the waveport. This is done to avoid spurious reflections. To excite the circularly polarized (CP) antenna, the two ports were fed with voltages of the same magnitude and with 90^{o} phase difference.

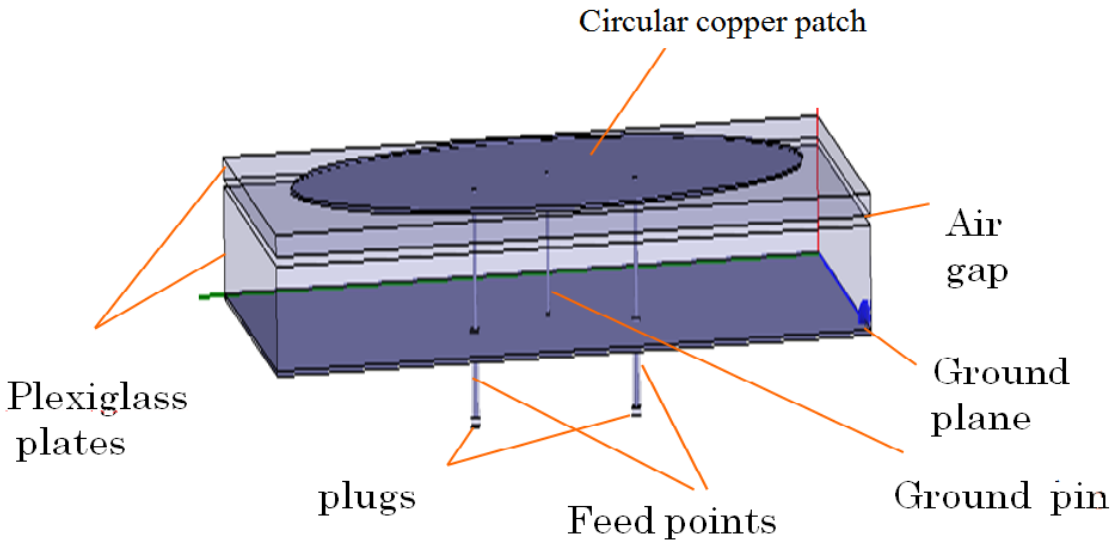

Figure 4: HFSS computer model of patch antenna

4.1 Patch Antenna in Free Space

For calculating in HFSS the mode-based scatting parameters of passive, high-frequency structures, a solution type of Driven Modal should be set before draw the antenna model. Since HFSS is a Finite-Element based method, a virtual object should be created to represent the radiation boundary to analyze radiation effects. For this antenna model, a radiation-transparent air volume surface which is a vacuum box outside the antenna (Figure 5) was created.

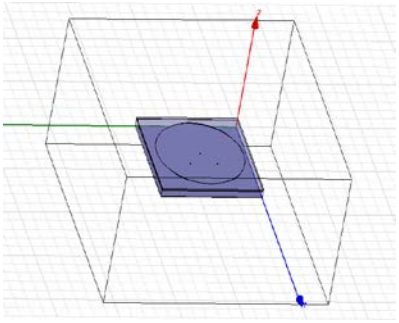

Figure 5: Antenna in vacuum box

According to previous MRI experimental work, the operating solution frequency should be centered around 298MHz and the sweep frequency range is from 200MHz to 400MHz. Due to its geometry, the S_{11} and S_{22} parameters of this antenna in free space are the same and are shown in Figure 6(a).

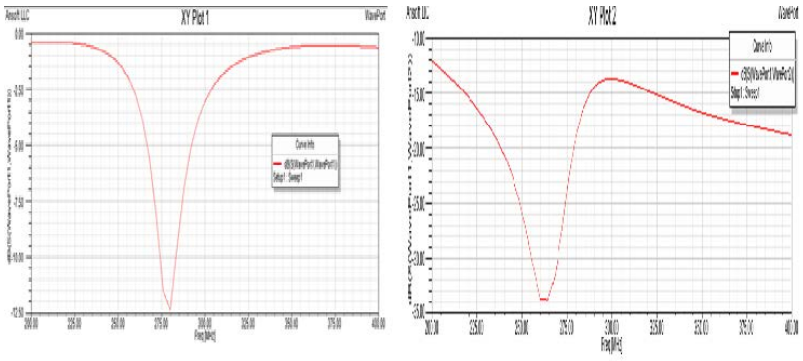

Figure 6: (a) HFSS data of $S_{11}$and S_{22} (antenna in free space)

(b) HFSS data of S_{12} and S_{21} (antenna in free space)

From Figure 6(a), it can be observed the antenna is matched to 50 Ω at 280MHz with a reflection coefficient of -12.5dB (0.056). Because of reciprocity, S12 and S21are also the same and are depicted in Figure 6(b). From Figure 6(b), a reflection coefficient of -18dB (0.016) is observed at 280MHz. From these results, we can tell 92.8% of energy will be radiated and lost. Besides, the plot for input impedance of port1 and port2 (Figure 7) indicates that the parallel resonance of the antenna in free space is approximately at 268MHz.

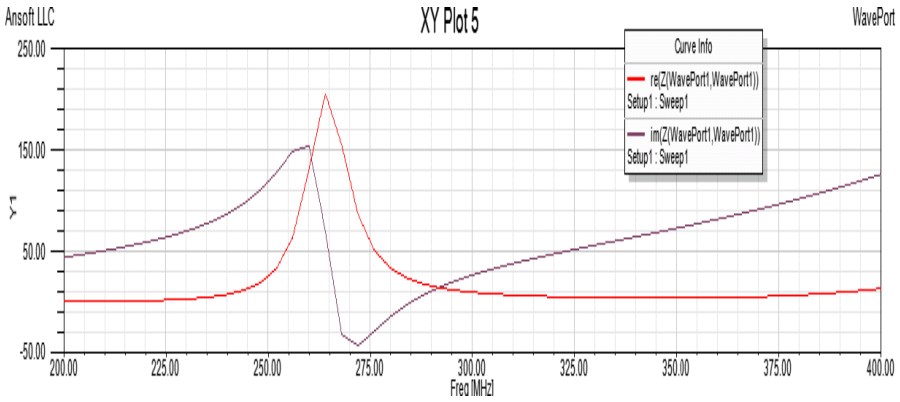

Figure 7: HFSS data of Z_{11} and Z_{22} (antenna in free space)

To study the far-field of the patch antenna in free space, the 3D radiation gain pattern is presented in Figure 8. As expected, a large main lobe points out in the broadside direction(+z axis) and is very symmetrical in the x-y plane.

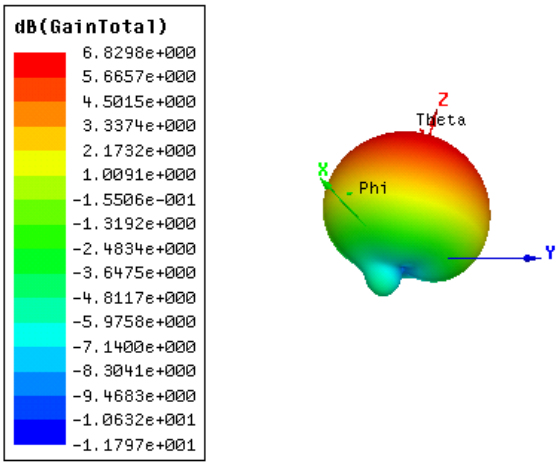

Figure 8: HFSS plot: radiation pattern (3D gain)

The plots of the radiation patterns (G_θ, $G_\emptyset$) in the x-z and y-z planes (Figure 9) are also similar, which proves that the antenna is symmetrical.

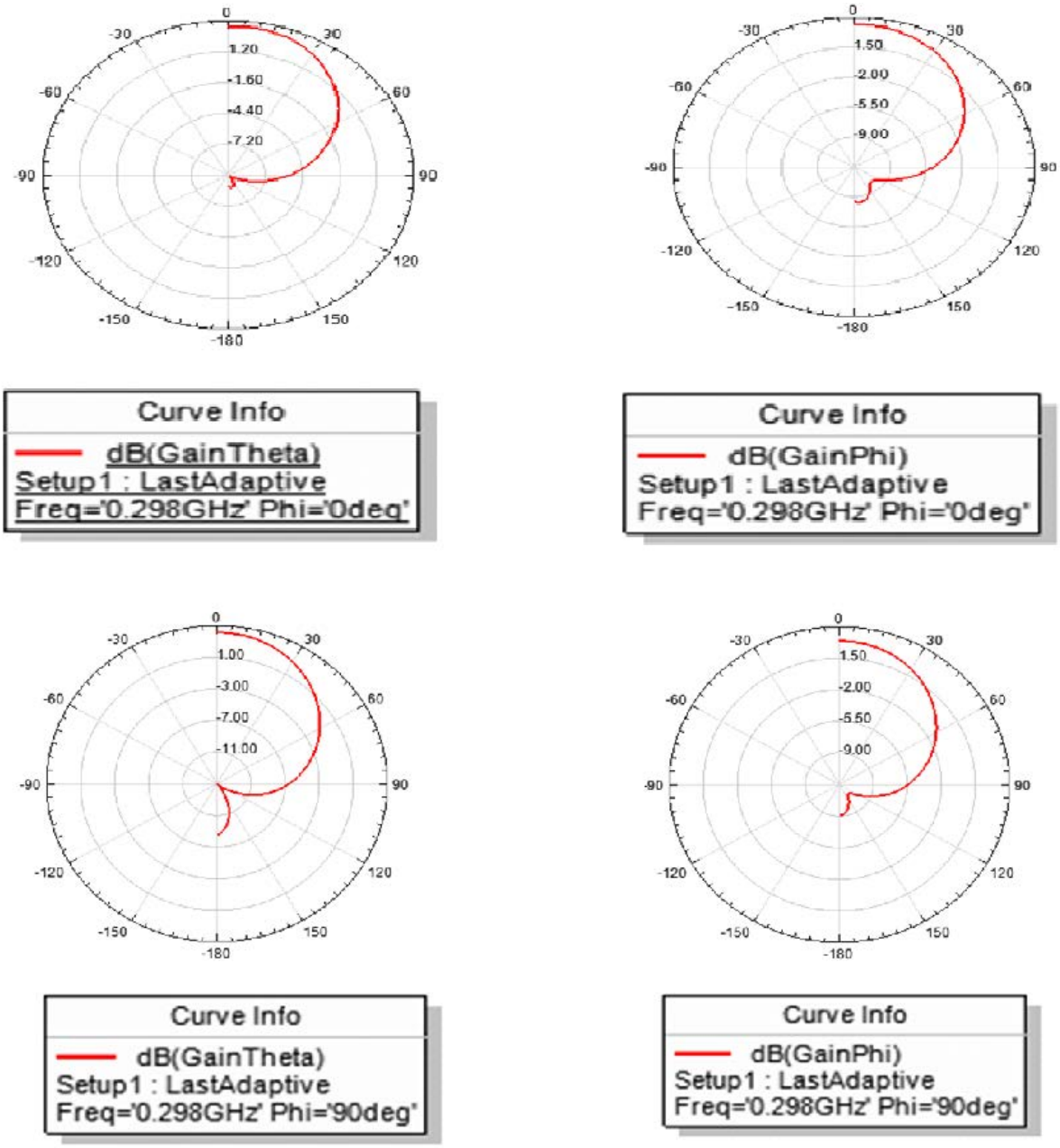

Figure 9: HFSS data: Radiation pattern (G_θ, $G_\emptyset$) in x-z plane and y-z plane

Since the ports of the antenna has been fed with 1 ∠0 ° (V) and 1 ∠90 ° (V), the right hand circularly polarized gain is much larger than its left hand circularly polarized gain (Figure 10).

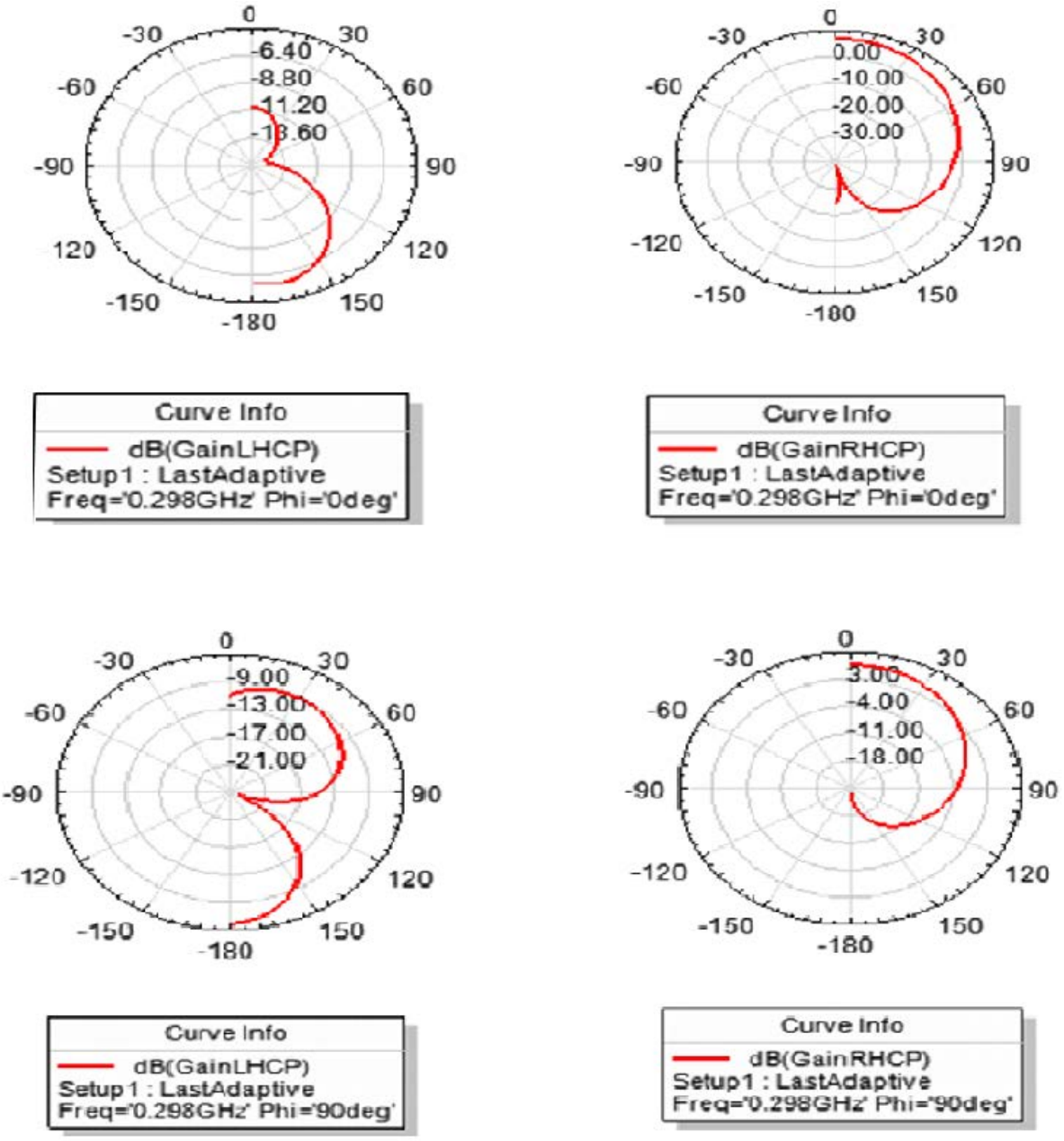

Figure 10: HFSS: Radiation pattern (G_{lhcp}, G_{rhcp}) in x-z plane and in y-z plane

Moreover, the axial ratio, the ratio of the magnitudes of the major and minor axis, is supposed to be one (0dB) for circular polarization. In Figure 11, the axial ratios above the x-y plane (theta=

[0°, 90°]) in the x-z and y-z plane are approximately 2dB (1.58). The reason for this may be related to the position of the feed points.

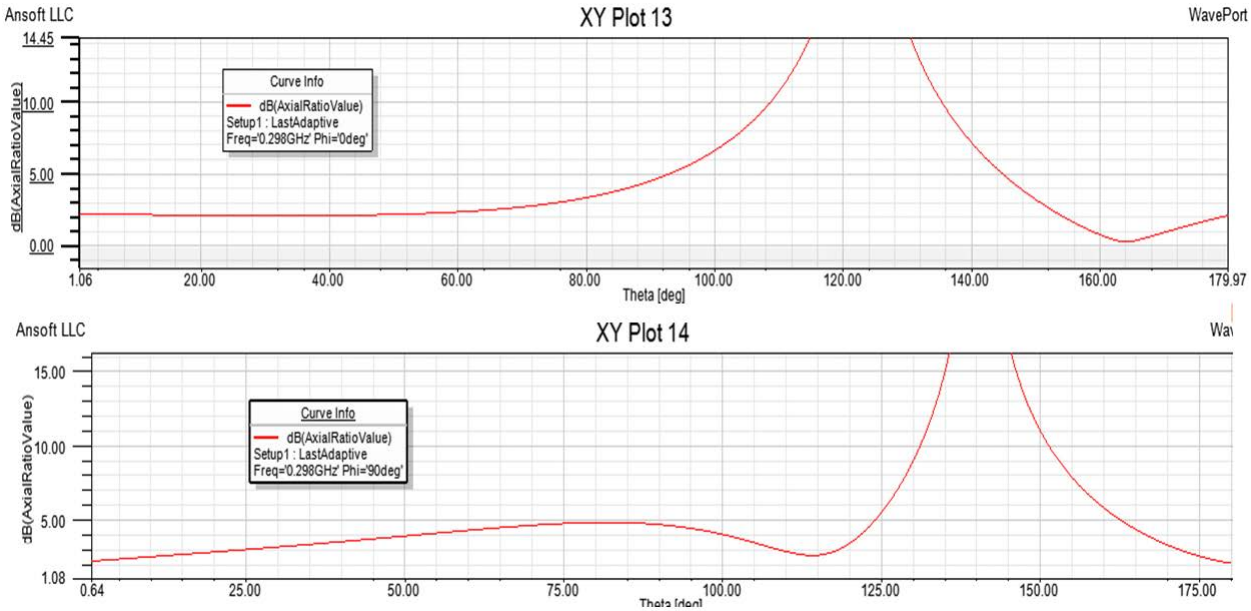

Figure 11: HFSS data: Axial Ratio in x-z plane and y-z plane

To compare with the experiment data measured previously, where a 3dB hybrid coupler is used to generate two signals in phase quadrature, the S-parameters calculated in HFSS can be exported to ADS where a 3dB hybrid coupler is added. A term port with 50 ohms was set to input signal which is equally split with a resultant 90 degree phase shift between outputs. The two outputs of hybrid coupler are connected with S2P (a System-Data Model) that can import S parameters solution data from HFSS. A 50 ohms resistor was added at the ISO port to maintain high isolation between the two output signals. S-parameters and Z_{in} at the input port can then be calculated in the frequency range from 200MHz to 400MHz. The schematic of the 3dB hybrid coupler is shown in Figure 12.

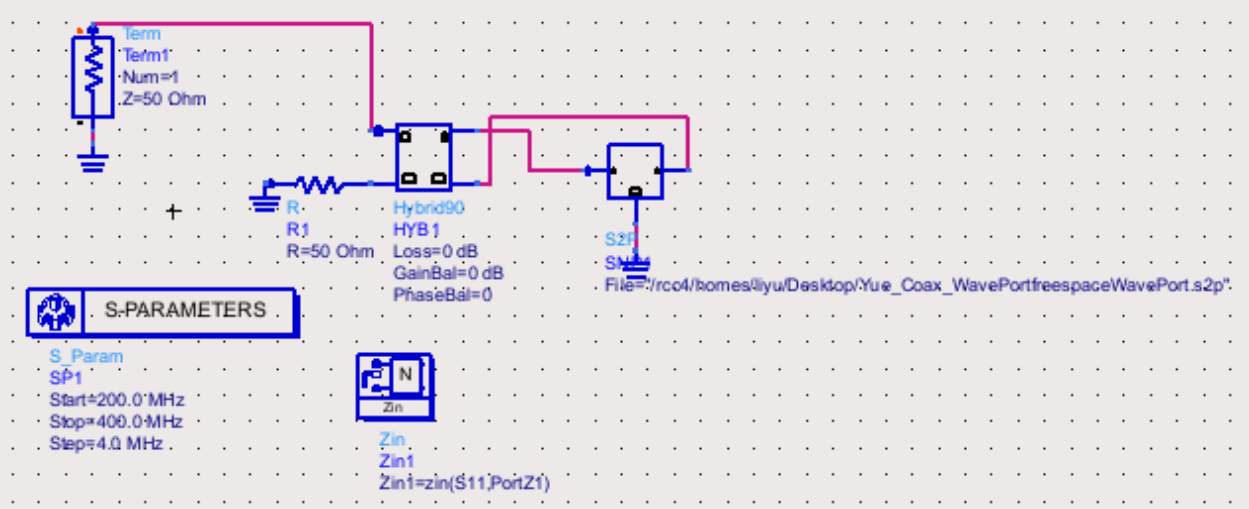

Figure 12: ADS: schematic of 3dB hybrid coupler

From ADS, the S_{11} plot (Figure 13) indicates that the antenna is matched to 50Ω at 263MHz which is a lower frequency smaller than a previously measured data (298MHz)[1]. The shift is most likely due to the nonuniform air gap between the two plexiglasses in the actual antenna. Our model assumes a uniform gap.

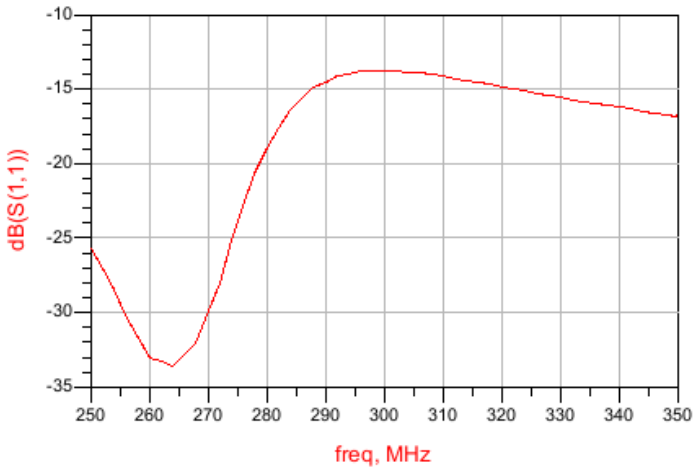

Figure 13: ADS data of S_{11} (antenna in free space)

Furthermore, the antenna has parallel resonance around 293MHz. The reactance is positive at these frequencies because of the extra inductance from the two probes feeding the antenna. Also, the patch antenna has two feeds and both ports have some mutual coupling. This implies that the driving point impedance depends on Z_{11} (=Z_{22}) and Z_{12} (Z_{21}) plus the input currents which are equal in magnitude but 90 degrees out of phase. The dip instead of peak in the real part is due to this coupling and phase quadrature of the input signals.

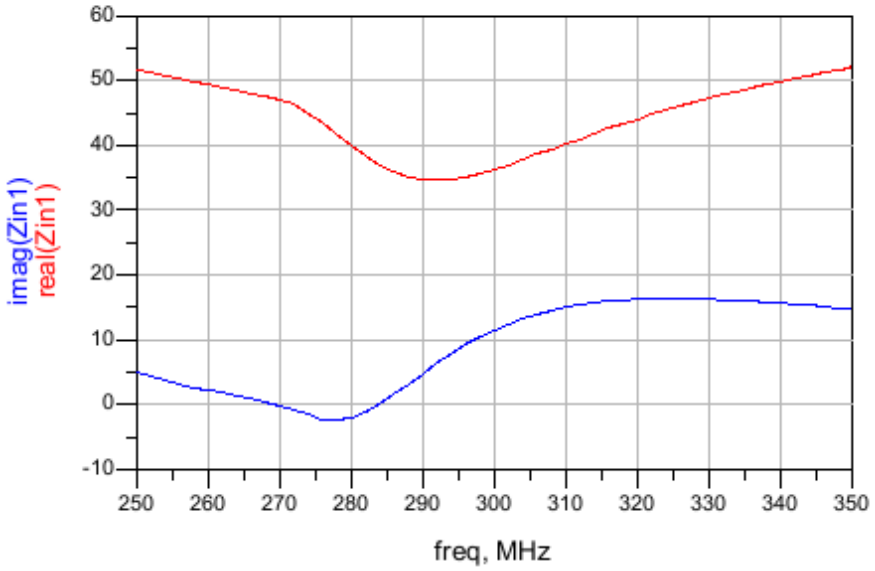

Figure 14: ADS data of Z_{11} (antenna in free space)

4.2 Patch Antenna in Empty Waveguide

To study the radiation properties of the patch antenna in an empty waveguide, the patch antenna is put in an empty cylinder (Figure 15) with Perfect electrical conducting (PEC) surface and two perfect matched layers at the terminal to absorb radiation energy. To simulate the bore of MRI, the cylinder is set as 2 meters long with 60cm in diameter.

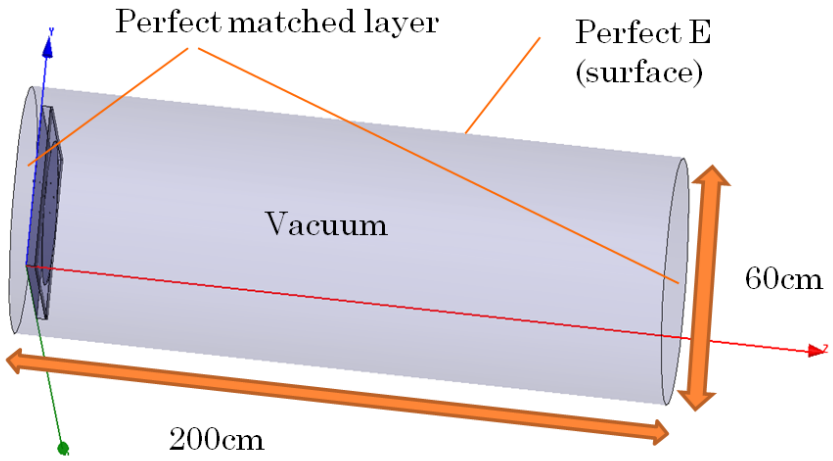

Figure 15: Computer model of patch antenna in empty waveguide

Cutoff frequencies for different TE or TM modes in free space ($\varepsilon_r = \mu_r = 1$) should be calculated based on this geometry. $P'nm$ in TE modes should be replaced by Pnm in TM modes. (a = the radius of cylinder)

$$f_{cutoff} = \frac{P'nm}{2\pi a\sqrt{\varepsilon\mu}} = \frac{P'nm}{2\pi a\sqrt{\mu_0\varepsilon_0}} = \frac{c*P'nm}{2\pi a}$$

To get the first three lowest cutoff frequencies for TE modes and TM modes, the first three smallest $P'nm$ or Pnm should be picked. The results are provided in Table 1. From Table1, only the cutoff frequency of TE_{11} mode is lower than our solution frequency 298 MHz. Thus, only TE_{11} mode will propagate and others will die out quickly.

nm	TE Mode	TM Mode
01	610MHz	383MHz
11	293MHz	610MHz
21	486MHz	817MHz

Table 1: First three lowest cutoff frequency in TE modes and TM modes

When the patch antenna is put inside an empty waveguide, the antenna is matched to 50 Ω at 308MHz with much larger reflection coefficients S_{11}/ S_{22} (Figure 16a) and S_{12}/ S_{21} (Figure 16b)). The perfect electrical conducting surface of an empty waveguide changes the near field of the antenna, so that its S parameters and input impedance increase dramatically due to its high sensitivity.

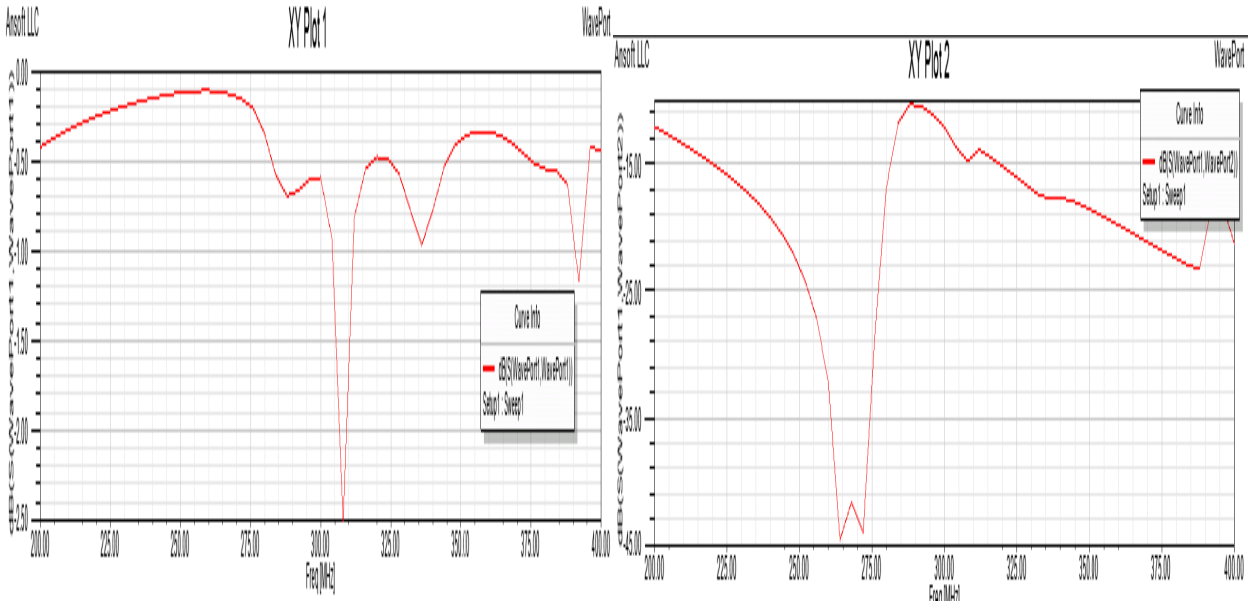

Figure 16: (a) HFSS data of S_{11} and S_{22} (antenna in an empty waveguide)

(b) HFSS data of S_{12} and S_{21} (antenna in an empty waveguide)

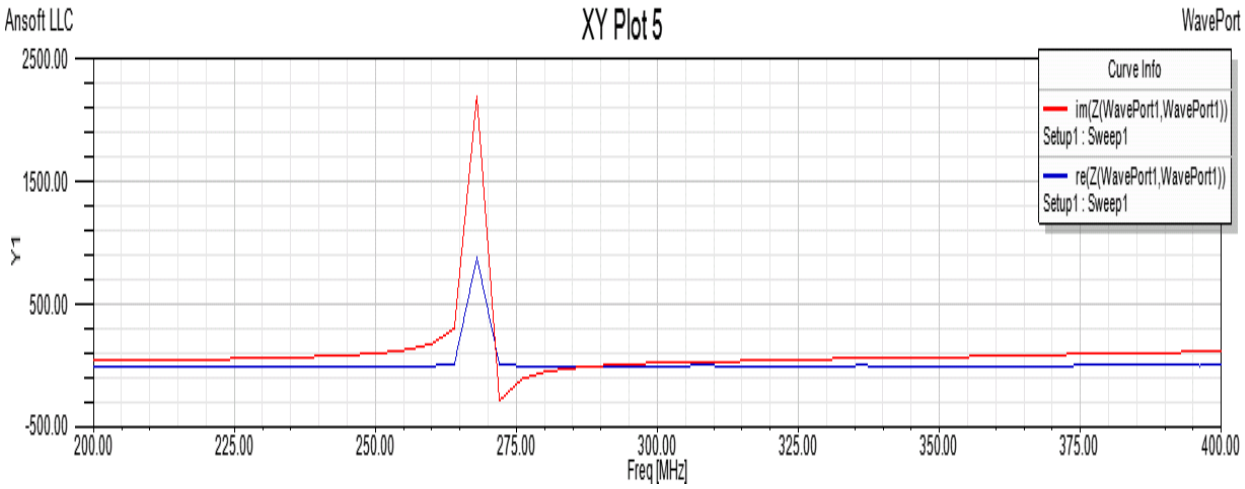

Figure 17: HFSS data of Z_{11} and Z_{22} (antenna in an empty waveguide)

The electrical (E) field distribution on the cross section of near field and after propagation illustrate that the E field closes to the two feed points is stronger than other place and the pattern after propagation is similar to that of TE_{11} mode.

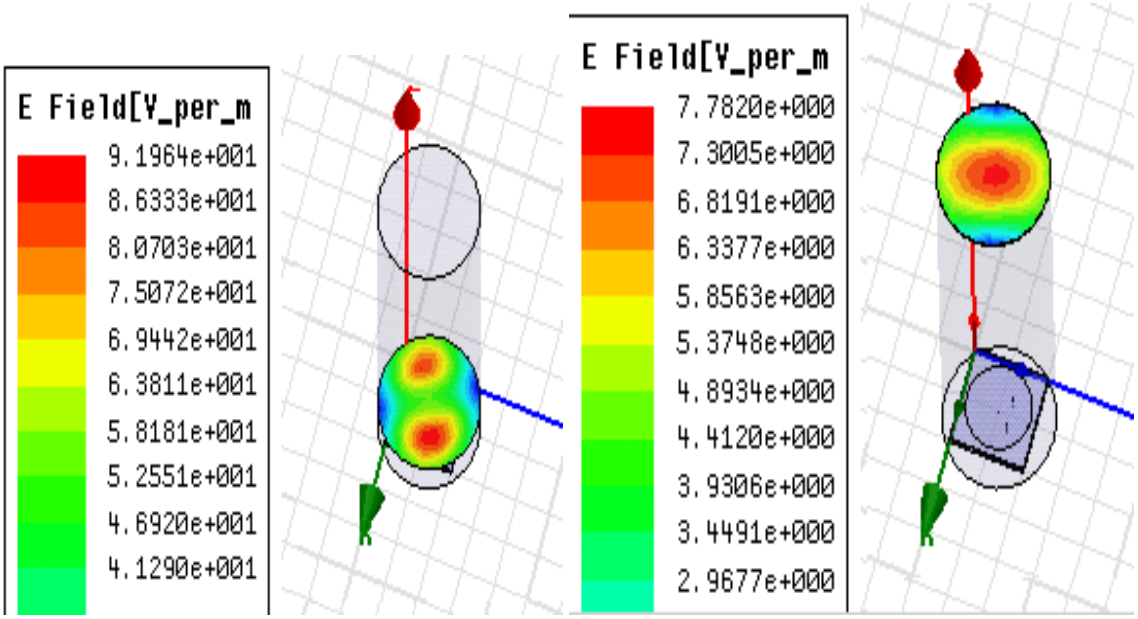

Figure 18: (a) HFSS: Electrical Field distribution in an empty waveguide (near field)

(b) HFSS: Electrical Field distribution in an empty waveguide (after propagation)

To investigate the effect after putting the patch antenna inside an empty waveguide, the solution data of S parameter from HFSS should be imported in the schematic (Figure 12). Comparing S_{11} (Figure 19) and Z_{11} (Figure 20) from ADS with those in free space, people can find out that they are approximately the same, respectively. Slightly different, both the real and imaginary part of input impedance is shifted down after antenna is put inside an empty waveguide. However, its parallel resonance remains the same.

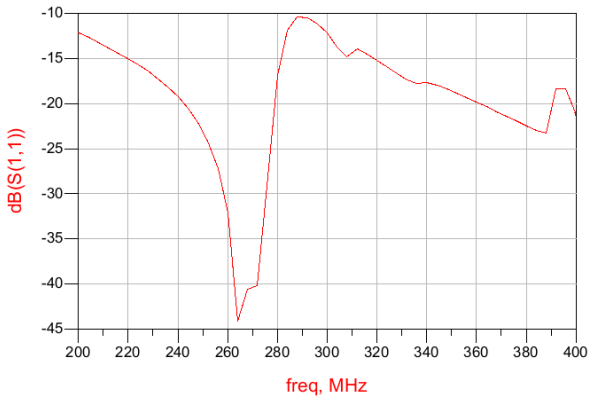

Figure 19: ADS data of S_{11} (antenna in empty waveguide)

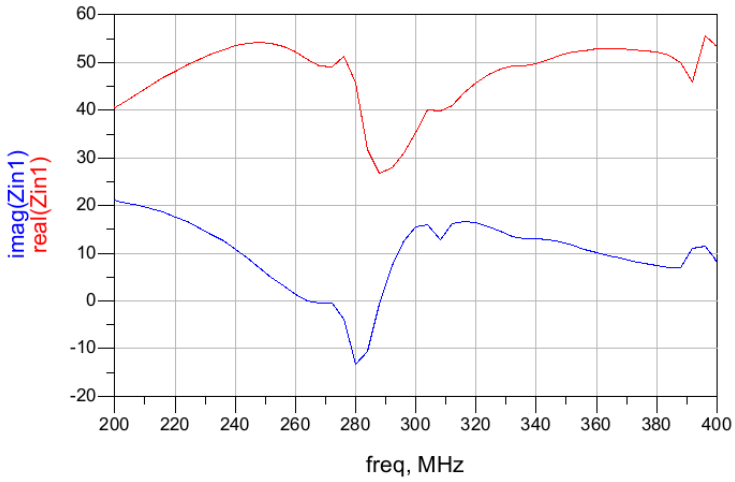

Figure 20: ADS data of Z_{11} (antenna in empty waveguide)

4.3 Patch Antenna in Waveguide with Phantom

To simulate a human body in MRI with waveguide exciter (Figure 21a) to excite traveling EM wave, a human-size phantom (Figure 21b) is placed in the middle of an empty waveguide. The human-size phantom is a cylinder with 160cm long and 40cm in diameter. According to previous experimental work, the phantom has relative permittivity $\varepsilon_r = 56.7$ and conductivity σ=0.94Sm^{-1}.

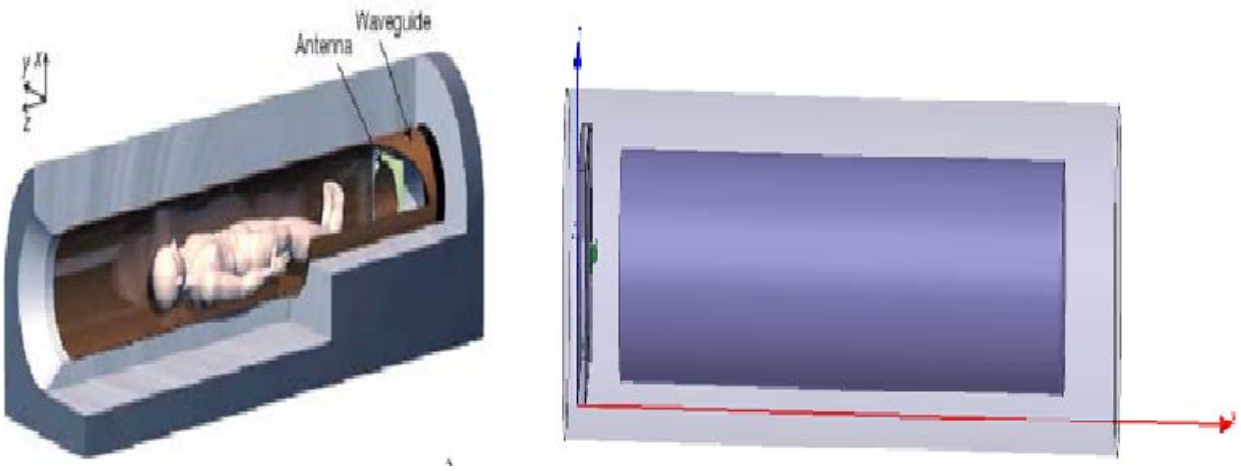

Figure 21: (a) Waveguide exciter to excite traveling EM waves in MRI [2]

(b) Computer model of patch antenna in a waveguide with a phantom

After the phantom was set inside the empty waveguide, the antenna is matched to 50 Ω at 292MHz, which is higher than that in free space. At 292MHz, the reflection coefficients S_{11}/ S_{22} (-16dB, Figure 22a) and S_{12}/ S_{21} (-18dB, Figure22b) are small, so around 90% of energy will be radiated or lost.

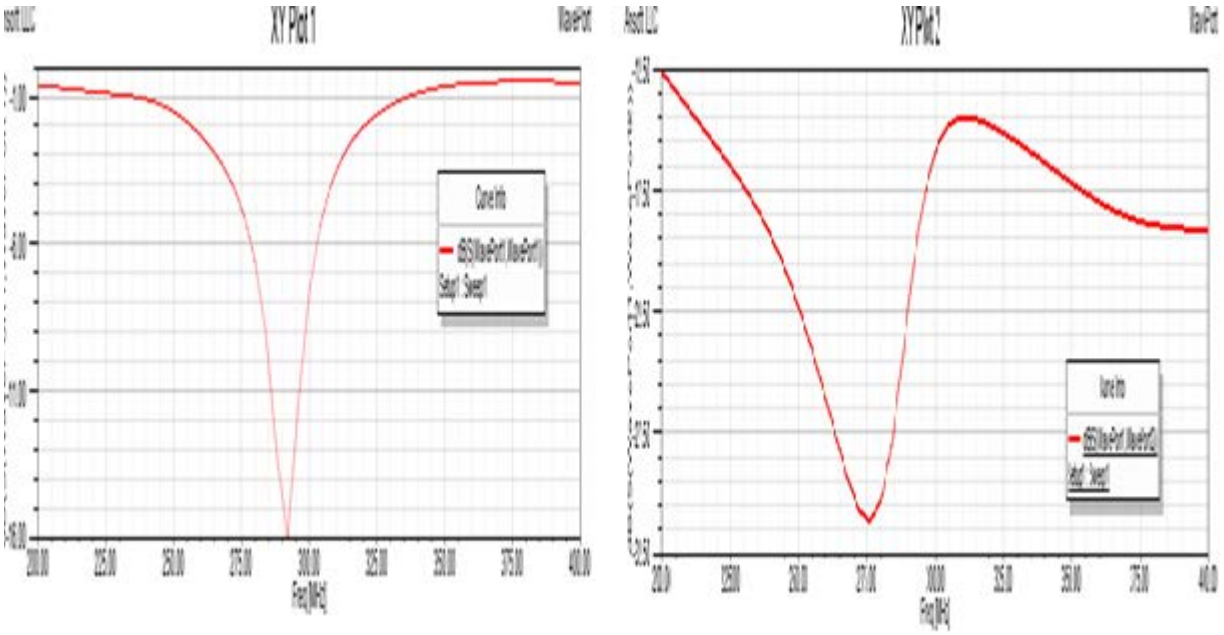

Figure 22: (a) HFSS data of S_{11} and S_{22} (antenna in a waveguide with a phantom)

(b) HFSS data of S_{12} and S_{21} (antenna in a waveguide with a phantom)

The resonance frequency is around 283MHz which is higher than that in free space.

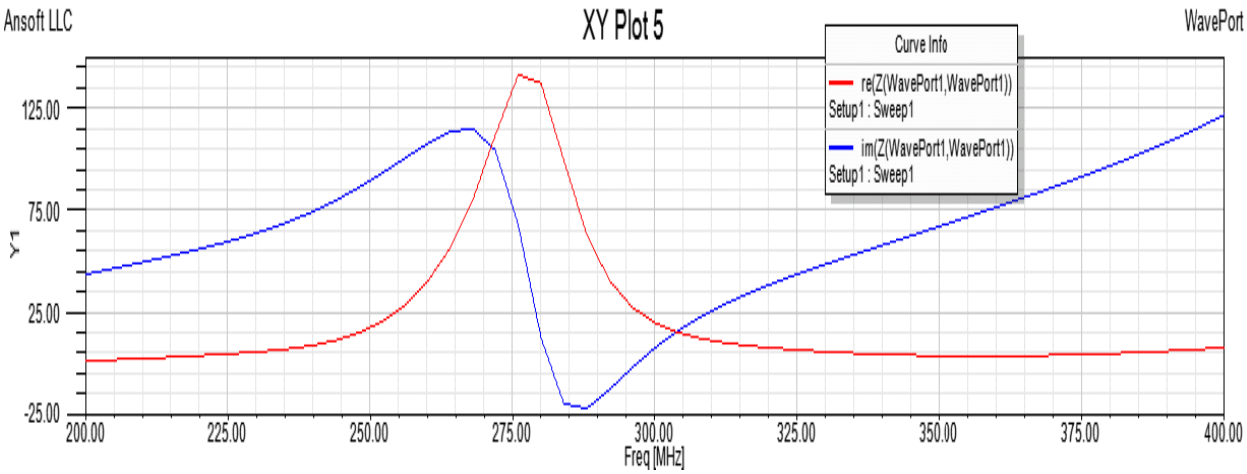

Figure 23: HFSS data of Z_{11} and Z_{22} (antenna in a waveguide with a phantom)

With the phantom inside a waveguide, the electrical field (Figure 24) is stronger than that in an empty waveguide. Its cross section pattern is distorted from the one with antenna in an empty waveguide after propagation.

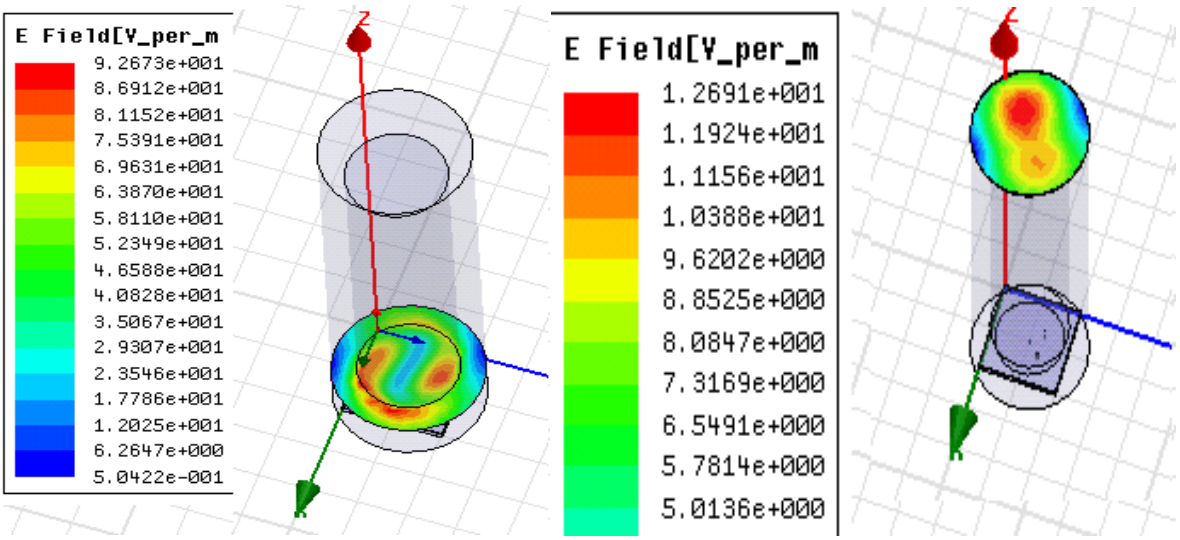

Figure 24: (a) HFSS: Electrical Field distribution in a waveguide with a phantom (near field)

(b) HFSS: Electrical Field distribution in a waveguide with a phantom (after propagation)

When comparing with S_{11} from ADS in an empty waveguide, people can figure out that the antenna is matched to 50Ω at 275 MHz which is higher than that without the phantom, which is closer to the previous measured results (298MHz). After the phantom has been put inside the waveguide, the near field of the antenna will be changed. Hence, the parallel resonance is shifted to 302MHz.

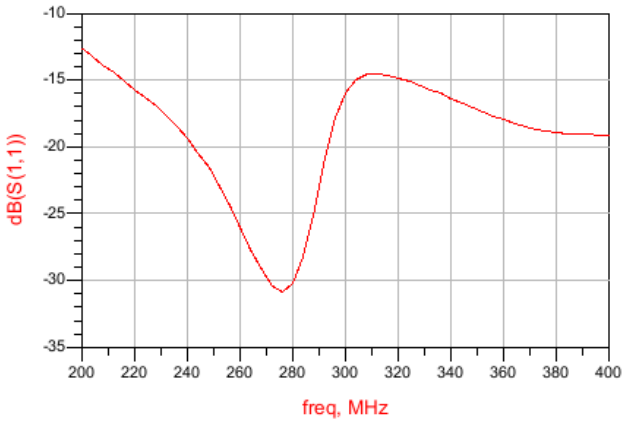

Figure 25: ADS data of S_{11} (antenna in a waveguide with a phantom)

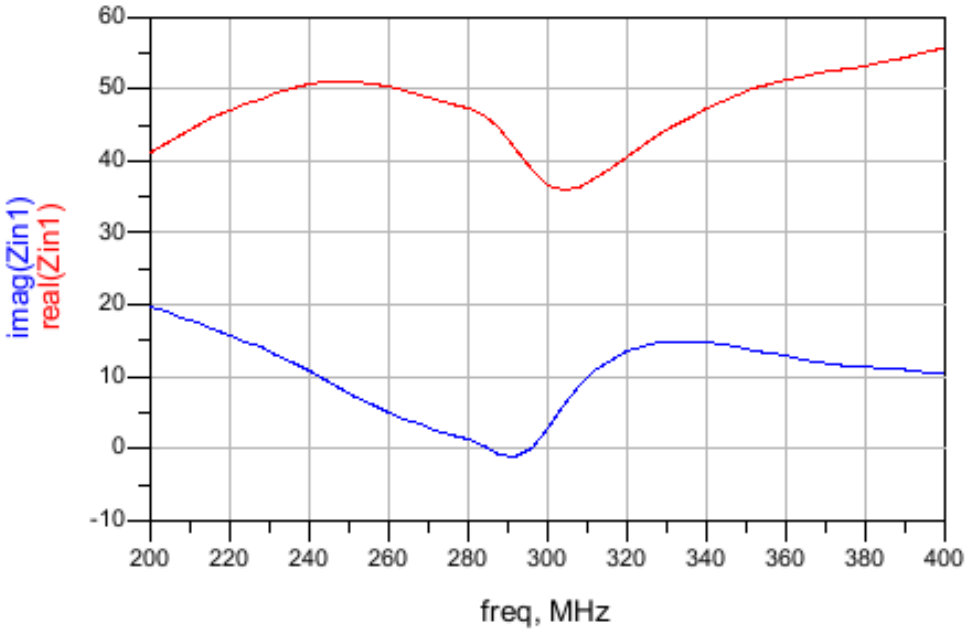

Figure 26: ADS data of Z_{11} (antenna in a waveguide with a phantom)

5.0 Related Studies

In view of the computer model of patch antenna in an empty waveguide, some related studies have been done to investigate the current antenna design method.

5.1 Comparison with Different Polarizations

In previous work, The RF pulse propagating as a circularly polarized wave through the bore of the scanner other than linearly polarized is mainly to reduce malicious standing wave which can cause distortion [2].

The electrical field generated in HFSS by circularly polarized wave and linearly polarized wave was explored by comparing their distribution pattern both near field and after propagation. The pattern of electrical field excited by linearly polarized wave is weaker and less symmetric than that of E field excited by circularly polarized wave. After propagation, the E field generated by linearly polarized wave is not as strong as that generated by circularly polarized wave. Therefore, circular polarization is a better choice than linear polarization for exciting the waveguide.

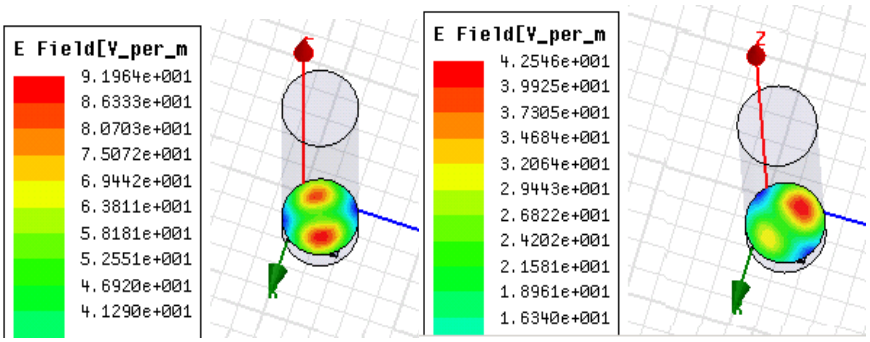

Figure 27: Circular polarization (left): Electrical field distribution (near field)

Linear polarization (right): Electrical field distribution (near field)

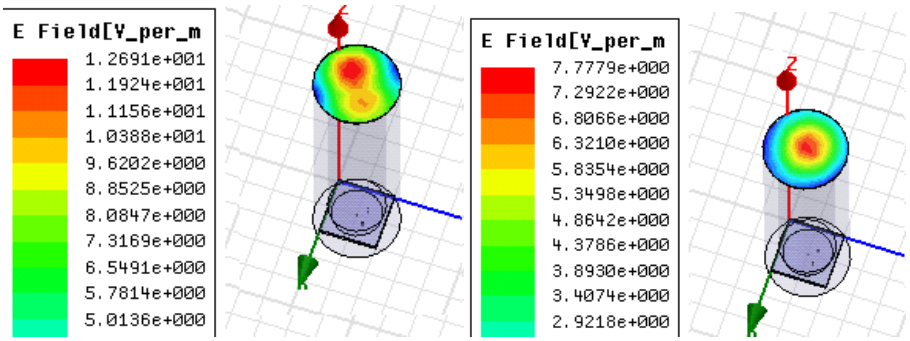

Figure 28: Circular polarization (left): Electrical field distribution (after propagation)

Linear polarization (right): Electrical field distribution (after propagation)

5.2 Comparison of Antenna Positions

From my design and results, some differences on scatting parameters and input impedance exists when the patch antenna was set in free space and in an empty waveguide. The determination of antenna position have been done by simulating its experimental S parameter and Z parameter in ADS with the patch antenna moved along positive z direction.

Figure 29 and Figure 30 represent the S parameter and the input impedance of the patch antenna when it was set at z=0cm, z=5cm and z=15cm. There is nearly no change shown as the patch antenna moved inside a waveguide. So, the position of patch antenna will not affect its MRI signals.

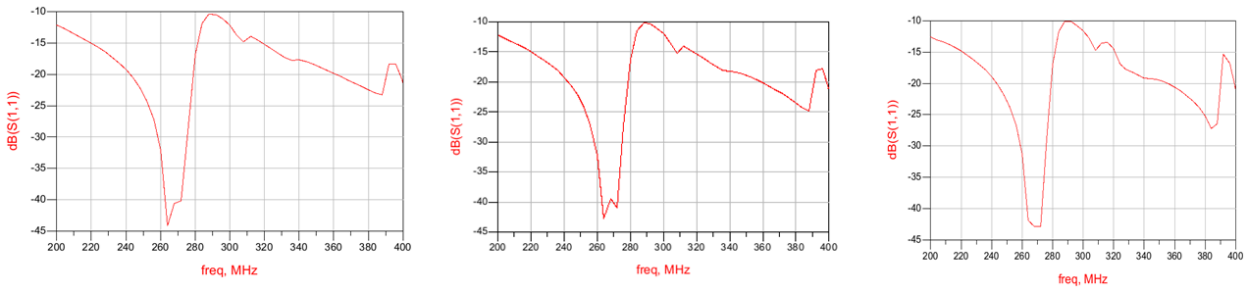

Figure 29: S_{11} in ADS when antenna position at z=0cm (left), z=5cm (middle), z=15cm (right)

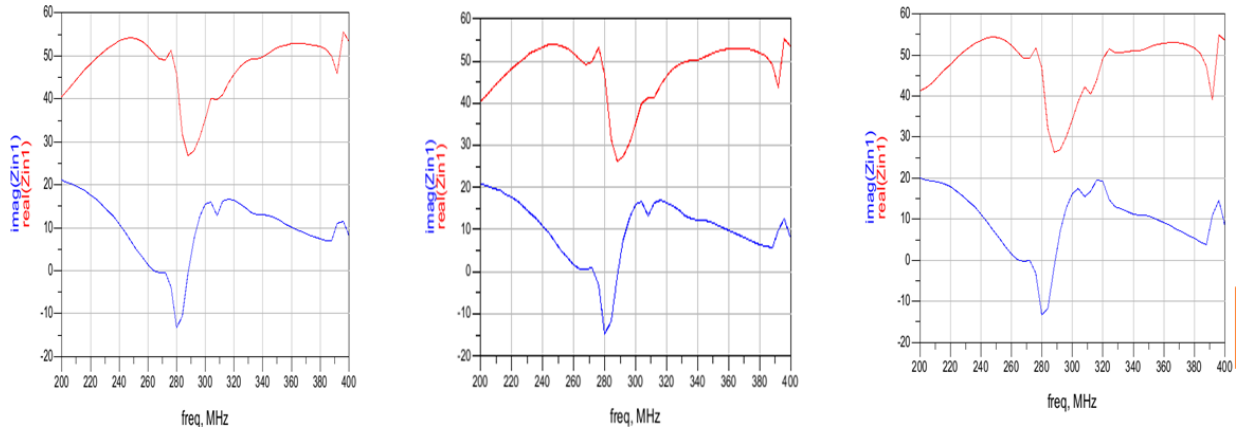

Figure 30: Z_{11} in ADS when antenna position at z=0cm (left), z=5cm (middle), z=15cm (right)

5.3 Comparison with Different Frequencies

According to calculation of cutoff frequencies for this MRI waveguide, the cutoff frequency of TE_{11} mode and TM_{11} mode are 293MHz and 383MHz, respectively. They are the two lowest cutoff frequencies for this geometry, meaning that no mode can propagate below 293MHz and both modes will propagate above 383MHz. Solution frequencies at 250MHz, 298MHz and 400MHz were picked to study its E field distribution both near field and after propagation.

The near field pattern (Figure 31) of electrical field distribution indicates that solution frequency at 298MHz can excite the strongest and most symmetrical electrical field. After propagation, all the modes should die out if the solution frequency is 250MHz which is lower than all the cutoff frequencies. Even though there is still some pattern in Figure32 (left), the maximum magnitude of E field is 1.25E-4 which is small enough to ignore. In Figure 32 (middle), only the pattern of TE_{11} mode can be found. And, a combination of patterns TE_{11} and TM_{11} modes has been got when solution frequency is 400MHz in figure 32 (right).

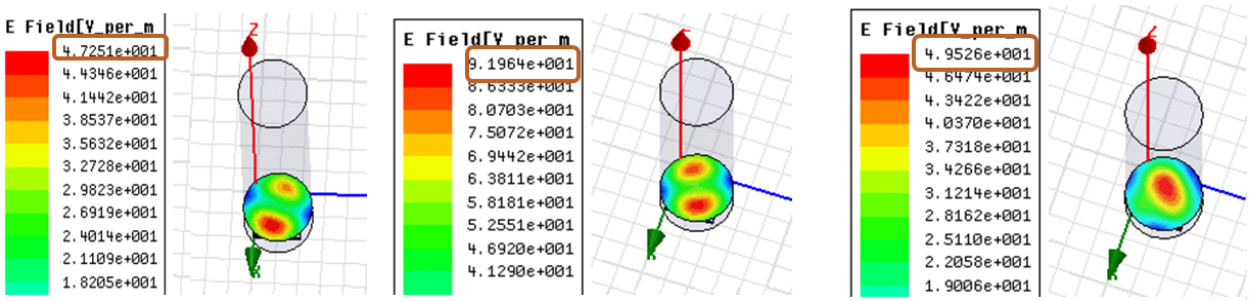

Figure 31: Electrical field distribution (near field) at 250MHz (left);

Electrical field distribution (near field) at 298MHz (middle);

Electrical field distribution (near field) at 400MHz (right);

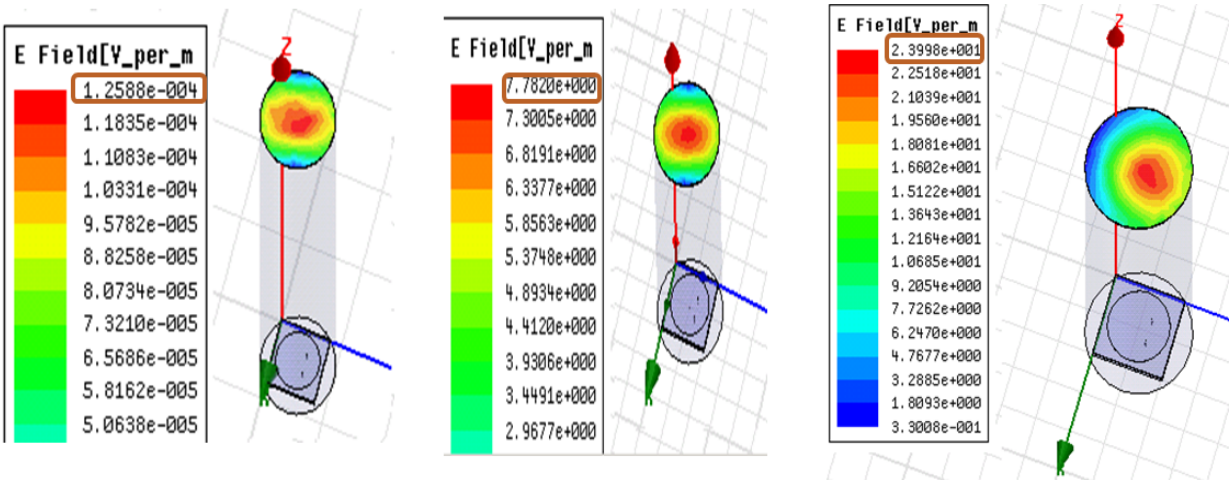

Figure 31: Electrical field distribution (after propagation) at 250MHz (left);

Electrical field distribution (after propagation) at 298MHz (middle);

Electrical field distribution (after propagation) at 400MHz (right);

6.0 Calculations

Since a gyrotropic material cannot be modeled in a HFSS waveguide, the near fields of the antenna located in an empty MRI bore can be first obtained in HFSS. These near fields of the antenna are then exported for calculation of the excitation coefficients. As mentioned before, these excitation coefficients are then used in COMSOL to simulate the response of the MRI traveling wave system to each mode individually. Assuming linearity, the total response is obtained by adding the response of the system to each mode.

The electrical field propagating in +z direction can be expressed as:

$$\vec{E} = \sum_{n}\sum_{m} C_{nm}\, \overrightarrow{e_{nm}} e^{-j\beta_{nm}z}$$

where Cnm = excitation coefficient, $\overrightarrow{e_{nm}}$=propagation mode,

$$\beta_{nm} = (k_0^2 - \frac{p_{nm}^2}{a^2})^{1/2}$$

To get the excitation coefficients, the following formula was used:

$$C_{nm} = \frac{\iint_S (\vec{E} \times \overrightarrow{h_{nm}}) \cdot \hat{z} dS}{\iint_S \overrightarrow{e_{nm}} \times \overrightarrow{h_{nm}} \cdot \hat{z} dS}$$

$$= \frac{\sum\sum(E_x * h_y - E_y * h_x)}{\sum\sum(e_x * h_y - e_y * h_x)}$$

where Ex and Ey are matrices of E field vector (near field) from HFSS

A grid should be generated to export the HFSS data of E field vector near the patch antenna. The side length of this grid is 0.004m which is smaller than λ/20. Because the cross section of exported electrical field is circular, zeros should be filled in the place where no E field vector existing. Two excitation coefficients should be determined for each mode due to the two cases to

calculate H plane propagation mode. The Matlab codes to calculate C_1 and C_2 of TE_{11} mode and TM_{11} mode are shown as follows:

TE_{11} mode (C_1):

```
clear all;
close all;
A = xlsread('waveportExreal.xlsx');
[X1,Y1] = meshgrid(-0.0718:.05:0.4782);
EXR= A(2:13,2:13);
[XI,YI] = meshgrid(-0.0718:.001:0.4782);
Exr = interp2(X1,Y1,EXR,XI,YI,'spline');
B = xlsread('waveportEximag.xlsx');
EXI= B(2:13,2:13);
Exi = interp2(X1,Y1,EXI,XI,YI,'spline');
C = xlsread('waveportEyreal.xlsx');
EYR= C(2:13,2:13);
Eyr = interp2(X1,Y1,EYR,XI,YI,'spline');
D = xlsread('waveportEyimag.xlsx');
EYI= D(2:13,2:13);
Eyi = interp2(X1,Y1,EYI,XI,YI,'spline');
%syms nu z
%Jd=diff(besselj(nu,z))
[X,Y]=meshgrid(-.0718:.001:0.4782,-.0718:.001:.4782);
[THETA,RHO]=cart2pol(X,Y);
n=1;
P11e=1.841;
a=0.03;
f=2.98*10^9;
c=3*10^8;
Kc11=P11e/a;
K0=2*pi*f/c;
Beta11=sqrt(K0^2-Kc11^2);
Ex=Exr+i*Exi;
Ey=Eyr+i*Eyi;
Z=P11e/a*RHO;
J=besselj(n,Z);
Jd=(1*besselj(n, Z))./Z - besselj(n, Z);
C=cos(THETA*n);
S=sin(THETA*n);
W=ones(551,551);
Hrho=-i*Beta11*P11e/a/Kc11^2*Jd.*C;
Htheta1=-i*n*Beta11/Kc11^2*W./RHO;
Htheta2=Htheta1.*J;
Htheta=Htheta2.*(-1)*S;
CC=cos(THETA);
SS=sin(THETA);
Hx1=CC.*Hrho;
Hx2=SS.*Htheta;
Hx=Hx1-Hx2;
Hy1=SS.*Hrho;
Hy2=CC.*Htheta;
Hy=Hy1+Hy2;
```

```
Num=Ex.*Hy-Ey.*Hx;
NUM=sum(sum(Num));
Z0=377;
Zh=K0*Z0/Beta11;
Den=Zh*Hy.*Hy+Zh*Hx.*Hx;
DEN=sum(sum(Den));
C1e=NUM/DEN
```

TE_{11} mode (C_2):

```
clear all;
close all;
A = xlsread('waveportExreal.xlsx');
[X1,Y1] = meshgrid(-0.0718:.05:0.4782);
EXR= A(2:13,2:13);
[XI,YI] = meshgrid(-0.0718:.001:0.4782);
Exr = interp2(X1,Y1,EXR,XI,YI,'spline');
B = xlsread('waveportEximag.xlsx');
EXI= B(2:13,2:13);
Exi = interp2(X1,Y1,EXI,XI,YI,'spline');
C = xlsread('waveportEyreal.xlsx');
EYR= C(2:13,2:13);
Eyr = interp2(X1,Y1,EYR,XI,YI,'spline');
D = xlsread('waveportEyimag.xlsx');
EYI= D(2:13,2:13);
Eyi = interp2(X1,Y1,EYI,XI,YI,'spline');
%syms nu z
%Jd=diff(besselj(nu,z))
[X,Y]=meshgrid(-0.0718:.001:0.4782,-0.0718:.001:0.4782);
[THETA,RHO]=cart2pol(X,Y);
n=1;
P11e=1.841;
a=0.03;
f=2.98*10^9;
c=3*10^8;
Kc11=P11e/a;
K0=2*pi*f/c;
Beta11=sqrt(K0^2-Kc11^2);
Ex=Exr+i*Exi;
Ey=Eyr+i*Eyi;
Z=P11e/a*RHO;
J=besselj(n,Z);
Jd=(1*besselj(n, Z))./Z - besselj(n, Z);
C=cos(THETA*n);
S=sin(THETA*n);
W=ones(551,551);
Hrho=-i*Beta11*P11e/a/Kc11^2*Jd.*S;
Htheta1=-i*n*Beta11/Kc11^2*W./RHO;
Htheta2=Htheta1.*J;
Htheta=Htheta2.*C;
CC=cos(THETA);
SS=sin(THETA);
Hx1=CC.*Hrho;
Hx2=SS.*Htheta;
Hx=Hx1-Hx2;
Hy1=SS.*Hrho;
```

```
Hy2=CC.*Htheta;
Hy=Hy1+Hy2;
Num=Ex.*Hy-Ey.*Hx;
Num=sum(sum(Num));
Z0=377;
Zh=K0*Z0/Beta11;
Den=Zh*Hy.*Hy+Zh*Hx.*Hx;
DEN=sum(sum(Den));
C2e=NUM/DEN
```

TM_{11} mode (C_1):

```
clear all;
close all;
A = xlsread('waveportExreal.xlsx');
[X1,Y1] = meshgrid(-0.0718:.05:0.4782);
EXR= A(2:13,2:13);
[XI,YI] = meshgrid(-0.0718:.001:0.4782);
Exr = interp2(X1,Y1,EXR,XI,YI,'spline');
B = xlsread('waveportEximag.xlsx');
EXI= B(2:13,2:13);
Exi = interp2(X1,Y1,EXI,XI,YI,'spline');
C = xlsread('waveportEyreal.xlsx');
EYR= C(2:13,2:13);
Eyr = interp2(X1,Y1,EYR,XI,YI,'spline');
D = xlsread('waveportEyimag.xlsx');
EYI= D(2:13,2:13);
Eyi = interp2(X1,Y1,EYI,XI,YI,'spline');
Ex=Exr+i*Exi;
Ey=Eyr+i*Eyi;
%syms nu z
%Jd=diff(besselj(nu,z))
[X,Y]=meshgrid(-0.0718:.001:0.4782,-0.0718:.001:0.4782);
[THETA,RHO]=cart2pol(X,Y);
n=1;
P11m=3.832;
a=0.03;
f=2.98*10^9;
c=3*10^8;
Kc11=P11m/a;
K0=2*pi*f/c;
Beta11=sqrt(K0^2-Kc11^2);
Z=P11m/a*RHO;
Z0=377;
Ze=Beta11/K0*Z0;
J=besselj(n,Z);
Jd=(1*besselj(n, Z))./Z - besselj(n, Z);
C=cos(THETA*n);
S=sin(THETA*n);
W=ones(551,551);
Htheta=-i*Beta11*P11m/a/Kc11^2/Ze*Jd.*C;
Hrho1=i*n*Beta11/Kc11^2/Ze*W./RHO;
Hrho2=Hrho1.*J;
Hrho=Hrho2.*(-1)*S;
CC=cos(THETA);
SS=sin(THETA);
Hx1=CC.*Hrho;
```

```
Hx2=SS.*Htheta;
Hx=Hx1-Hx2;
Hy1=SS.*Hrho;
Hy2=CC.*Htheta;
Hy=Hy1+Hy2;
Num=Ex.*Hy-Ey.*Hx;
NUM=sum(sum(Num));
Den=Ze*Hy.*Hy+Ze*Hx.*Hx;
DEN=sum(sum(Den));
C1m= NUM/DEN
```

TM_{11} mode (C_2):

```
clear all;
close all;
A = xlsread('waveportExreal.xlsx');
[X1,Y1] = meshgrid(-0.0718:.05:0.4782);
EXR= A(2:13,2:13);
[XI,YI] = meshgrid(-0.0718:.001:0.4782);
Exr = interp2(X1,Y1,EXR,XI,YI,'spline');
B = xlsread('waveportEximag.xlsx');
EXI= B(2:13,2:13);
Exi = interp2(X1,Y1,EXI,XI,YI,'spline');
C = xlsread('waveportEyreal.xlsx');
EYR= C(2:13,2:13);
Eyr = interp2(X1,Y1,EYR,XI,YI,'spline');
D = xlsread('waveportEyimag.xlsx');
EYI= D(2:13,2:13);
Eyi = interp2(X1,Y1,EYI,XI,YI,'spline');
Ex=Exr+i*Exi;
Ey=Eyr+i*Eyi;
%syms nu z
%Jd=diff(besselj(nu,z))
[X,Y]=meshgrid(-0.0718:.001:0.4782,-0.0718:.001:0.4782);
[THETA,RHO]=cart2pol(X,Y);
n=1;
P11m=3.832;
a=0.03;
f=2.98*10^9;
c=3*10^8;
Kc11=P11m/a;
K0=2*pi*f/c;
Beta11=sqrt(K0^2-Kc11^2);
Z=P11m/a*RHO;
Z0=377;
Ze=Beta11/K0*Z0;
J=besselj(n,Z);
Jd=(1*besselj(n, Z))./Z - besselj(n, Z);
C=cos(THETA*n);
S=sin(THETA*n);
W=ones(551,551);
Htheta=-i*Beta11*P11m/a/Kc11^2/Ze*Jd.*S;
Hrho1=i*n*Beta11/Kc11^2/Ze*W./RHO;
Hrho2=Hrho1.*J;
Hrho=Hrho2.*C;
CC=cos(THETA);
```

```
SS=sin(THETA);
Hx1=CC.*Hrho;
Hx2=SS.*Htheta;
Hx=Hx1-Hx2;
Hy1=SS.*Hrho;
Hy2=CC.*Htheta;
Hy=Hy1+Hy2;
Num=Ex.*Hy-Ey.*Hx;
NUM=sum(sum(Num));
Den=Ze*Hy.*Hy+Ze*Hx.*Hx;
DEN=sum(sum(Den));
C2m= NUM/DEN
```

The result for both circularly polarized wave and linearly polarized wave are presented in Table 2. The excitation coefficients of potential propagating modes, with lower cutoff frequency, are much smaller, which is unexpected. Since the evanescent mode cannot propagate and would store energy, the excitation coefficients of propagating modes are supposed to be much larger to radiate more energy. In consequence, the patch antenna should be redesigned.

	Circularly Polarized		Linearly Polarized	
	C1	C2	C1	C2
TE11	-0.0193+0.0041i	-0.016+0.012i	-0.0095+0.0050i	-0.0138+0.0091i
TM01	-1.3839+0.8874i	-	-0.1114+0.2531i	-
TE21	0.0236-0.0915i	-0.0052+0.0012i	0.063-0.0474i	-0.0055+0.0038i
TM11	16.4976-61.8568i	-0.0608-3.6056i	-22.4004-51.0758i	-1.9641-3.4882i

Table 2: Excitation coefficients for several modes excited by circularly polarized wave and linearly polarized wave

7.0 Summary and Conclusion

An accurate computer model of a circularly polarized patch antenna was developed in HFSS and several studies of the behavior of this antenna in free space, in an empty waveguide as well as in a waveguide with a phantom have been performed to explore the novel high field Magnetic Resonance Imaging traveling wave system.

Due to uniform air gap, the simulation results of match point and parallel resonance frequency are lower than that measured in previous experiment. As expected, approximate 90% of energy generated by the patch antenna can be radiated or lost instead of reflecting back to the ports. Also, the radiation pattern of the patch antenna excited by right hand circularly polarized wave is very symmetrical. Some differences on input impedance behavior and radiation properties illustrate high sensitivity of near field for the patch antenna. Furthermore, circular polarization is a better choice than linear polarization when exciting the waveguide. The position of patch antenna will not affect its MRI signal. Solution frequency at 298MHz can excite stronger and more symmetrical electrical field. Last, the excitation coefficients of evanescent mode are too large so that most energy will be stored. Future work should be done to redesign the antenna.

8.0 Future Work

A same size circular waveguide filled with gyrotropic materials [4] (body under test) can be built in Comsol. The waveguide needs to be excited by desired incident mode and power intensity (excitation coefficients) based on calculation data in Matlab. Finally, all the results for different modes should be summed up.

With this simulated results, the advantages and disadvantages of either one exciter at one end of the waveguide or an exciter at each of the two ends of the waveguide in the traveling wave MRI can be studied. Additionally, it will be important to determine the minimum distance of the phantom from the exciter as well as to develop exciter designs that are not very sensitive to the phantom (i.e. ultimately the human body in the MRI system).

Acknowledgements

I would like to express my sincere appreciation to Prof. Roberto G. Rojas-Teran for serving as my research advisor for an academic year and providing much guidance on my research. Thanks to Prof. Petra M. Schmalbrock to attend my oral thesis defense with Prof. Rojas and we had a good discussion. Furthermore, graduate student Renaud Moussounda helped and provided suggestions on patch antenna simulation. The College of Engineering also provided funding support as scholarship for the duration of the research project.

Bibliography

1. Hernandez, Zachary, "*The exploration of Traveling Waves in High Field Magnetic Resonance Imaging.*" Final Report for SROP Program, 2010
2. Brunner D.O., *et al*., "Traveling-wave nuclear magnetic resonance," Nature, Vol. 457, pp. 994-999, February 2009

3 Wexner Medical Center. *Why OSU*. Web. < http://radiology.osu.edu/11649.cfm>

4. Alshannaq, S. S and Rojas, R. G., "*Nonreciprocity in circular magnetoplasma-filled waveguides above the cyclotron frequency.*" Journal of Applied Physics 106,034502 (2009).